The EUMETSAT Satellite Application Facility on Land Surface Analysis

Validation Report

Down-welling Longwave Flux (DSLF)

PRODUCTS: LSA-10 (MDSLF), LSA-11 (EDSLF), LSA-12 (DIDSLF)

The EUMETSAT Network of Satellite Application Facilities

LSA SAF
Land Surface Analysis

Reference Number:	SAF/LAND/IM/VR_DSLF/I_11v1
Issue/Revision Index:	Issue I/2011 v1
Last Change:	12/04/2011

DOCUMENT SIGNATURE TABLE

	Name	Date	Signature
Prepared by :	I. Trigo, I. Monteiro, S. Freitas		
Approved by :	Land SAF Project Manager (IM)		

DOCUMENTATION CHANGE RECORD

Issue / Revision	Date	Description:
Version I/2011	12/04/2011	Section 5.2 now includes a comparison of daily DSLF (DIDSLF) with in situ observations.

DISTRIBUTION LIST

Internal Consortium Distribution		
Organisation	**Name**	**No. Copies**
IM	Pedro Viterbo	
IM	Luís Pessanha	
IM	Isabel Trigo	
IDL	Carlos da Camara	
IM	Isabel Monteiro	
IM	Sandra Coelho	
IM	Carla Barroso	
IM	Pedro Diegues	
IM	Teresa Calado	
IM	Benvinda Barbosa	
IM	Ana Veloso	
IMK	Folke-S. Olesen	
IMK	Frank Goettsche	
IMK	Ewa Kabsch	
MF	Jean-Louis Roujean	
MF	Olivier Hautecoeu	
MF	Dominique Carrer	
RMI	Françoise Meulenberghs	
RMI	Arboleda Alirio	
RMI	Nicolas Ghilain	
FMI	Niilo Siljamo	
UV	Joaquin Melia	
UV	F. Javier García Haro	
UV/EOLAB	Fernando Camacho	
UV	Aleixander Verger	

External Distribution		
Organisation	**Name**	**No. Copies**
EUMETSAT	Frédéric Gasiglia	
EUMETSAT	Dominique Faucher	
EUMETSAT	Lorenzo Sarlo	
EUMETSAT	Lothar Schueller	
EDISOFT	Teresa Cardoso	
EDISOFT	Carlos Vicente	
EDISOFT	Cleber Balan	
SKYSOFT	João Canário	

Steering Group Distribution		
Nominated by:	**Name**	**No. Copies**
IM	Carlos Direitinho Tavares	
EUMETSAT	Lorenzo Sarlo	
EUMETSAT	Yves Govaerts	
EUMETSAT	François Montagner	
STG/AFG (USAM)	Luigi de Leonibus	
MF	François Bouyssel	
RMI	Steven Dewitte	
FMI	Carl Fortelius	

Executive Summary

Downwelling Surface Long-wave radiative Flux (DSLF) is defined as the irradiance reaching the surface in the thermal infrared part of the spectrum (4-100 μm). The DSLF product for SEVIRI sensor is operational within the LSA SAF since the beginning of the CDOP, while a similar algorithm, adapted to AVHRR/MetOp, was integrated into the EPS chain in September 2007. A further product product, corresponding to the daily (0 – 24 UTC) accumulation of Meteosat instantaneous 30-minute fields, is also being processed regularly by the LSA SAF system parallel chain since August 2009 and, since July 2010, by the operational suite of MSG,

This document presents the most recent validation results obtained for the LSA SAF DSLF products. In the case of DSLF_SEVIRI, these are based on the comparison with ground observations, most of which available from the BSRN database. The validation of DSLF_SEVIRI suggests that a high percentage (generally over 60-to-70%) of estimated values meets the target accuracy of 10%. However, the results also point towards a systematic underestimation of DSLF in clear sky conditions, and high dispersion of Land-SAF versus in situ measurements in cloudy cases. This is particularly evident in Tamanrasset (in the Sahara). Such results lead to a further assessment of different bulk parameterizations of infrared downward fluxes at the surface, including: (i) two schemes applicable to clear sky conditions developed by Prata (1996) and Dilley and O'Brien (1998), respectively, and in use by the LSA SAF; (ii) the scheme first proposed by Josey et al. (2003), applicable to all sky conditions, and in use by the LSA SAF for cloudy cases only; and (iii) a generalized version of the formulation first proposed by Prata (1996), valid for all sky conditions. The latter was calibrated using data by simulated MODTRAN for the TIGR-like database (Chevallier et al., 2001).

The intercomparison of the above-mentioned parameterization schemes for DLSF clearly indicates that the DSLF formulation developed by the LSA SAF (hereafter designated by Prata_Modified or New_Parameterization scheme) is able to reduce systematic errors in both clear and cloudy sky conditions. Such formulation is currently used for operational generation of Meteosat DSLF. A similar code has been tested for EPS data in the parallel chain. The very first preliminary results obtained from a comparison with Meteosat DSLF are shown here.

The daily DSLF fields produced for the period between August and December 2009 are analysed for consistency. Generated fields and global statistics are compared to ECMWF forecasts of daily accumulated downward thermal fluxes. These are shown to share common features. Missing time-slots within the instantaneous (30-minute) DSLF fields are identified as the main contributors for the degradation of daily DSLF quality. The daily DSLF SEVIRI data are compared with the available ground observations from BSRN database for the 2010 period. Overall, the assessment against in situ measurements presents good results, with the exception of stations located in sites with difficult cloud classification from SEVIRI or not representative of the pixel scale.

TABLE OF CONTENTS

List of Tables

List of Figures

1 Introduction

Downwelling Surface Long-wave radiative Flux (DSLF) is defined as the irradiance reaching the surface in the thermal infrared part of the spectrum (4-100 μm). The DSLF product for SEVIRI sensor is operational within the LSA SAF since the beginning of the CDOP, available to users in near-real time (via EUMETCast) or offline (via ftp). A similar product is generated using data from AVHRR onboard MetOp since the 3rd quarter of 2007. The daily accumulation (0 – to – 24 UTC) of SEVIRI/Meteosat DSLF, DIDSLF, is also generated operationally on a regularly basis since July 2010. The fields are made available along with the percentage of missing time-slots through the period between 0 and 24 UTC, estimated on a pixel-by-pixel basis.

DSLF can only be indirectly inferred from remotely sensed data. In the approach used by the LSA SAF, DSLF is estimated using the signature of clouds and cloud types on IR and VIS channels, complemented with information on atmosphere water content and temperature profiles available from NWP fields. It is worth noting the latter, obtained from ECMWF forecasts with ranges between 12h and 24h, include information from atmospheric sounders and other observations, and thus correspond to the best knowledge of atmospheric profiles for each time-slot.

Both SEVIRI and AVHRR products use bulk parameterization schemes calibrated to clear and or cloudy pixels, respectively. The pre-requisites to the DSLF algorithm include 2m temperature, 2m dew point and total column water vapour (provided by ECMWF forecasts), and cloud information - Cloud Mask, Cloud Type, and Effective Cloudiness (provided by NWC SAF software, processed at IM). An automatic Quality Control (QC) is performed on DSLF data and the quality information is provided on a pixel basis. The DSLF QC contains general information about input data quality and information about DSLF confidence level.

User requests regarding DSLF are summarised in Table 1; further details may be found in the most recent version of the Product Requirements Table (PRT). The latest PRT version may be downloaded from the LSA SAF website http://landsaf.meteo.pt.

Table 1 Product Requirements for DSLF, in terms of area coverage, resolution and accuracy.

DSLF Product	Coverage	Resolution		Accuracy		
		Temporal	Spatial	Threshold	Target	Optimal
MDSLF (LSA-10): DSLF_SEVIRI	MSG disk	30 min	MSG pixel resolution	20%	10%	5%
EDSLF (LSA-11): DSLF_AVHRR	Europe & High Latitudes	1/2 day	0.01° x 0.01°	20%	10%	5%
DIDSLF (LSA-12): DSLF_DAILY	MSG disk	Daily	MSG pixel resolution	20%	10%	5%

This document presents the most recent validation results obtained for the LSA SAF DSLF products. In the case of DSLF_SEVIRI (section 2), these are based on the comparison with ground observations, most of which available from the BSRN

database. As will be shown in section 2, the first version of DSLF algorithm (based on Prata, 1996, and Josey et al, 2003 parameterizations) presented a relatively poor performance over Northern Africa, where in situ measurements are sparse. In order to improve the statistics of DSLF, particularly under cloudy conditions, the LSA SAF calibrated a new formulation of the Prata (1996) – hereafter Prata_Modified or New_Parameterization scheme – using a dataset of MODTRAN simulations for a wide range of atmospheric conditions. The 1st version of DSLF algorithm and the Prata_Modified DSLF values are validated against an independent dataset of in situ observations. The Prata_Modified is shown to reduce product bias and root mean square errors, particularly under cloudy conditions.

2 Downwelling Surface Long-wave Flux – Parameterizations

Several methods have been developed to estimate DSLF from top of atmosphere satellite observations. The LSA SAF makes use of a semi-empirical method to obtain DSLF every 30 minutes from Meteosat Second Generation TOA observations, on a pixel-by-pixel basis. DSLF is produced for the four geographical regions within MSG disk, up to viewing angles of 80º (e.g., Figure 1). The DSLF retrievals benefit from the signature of clouds and different cloud types on IR (Infrared) and VIS (Visible) channels, obtained from the Nowcasting SAF (NWC SAF; http://nwcsaf.inm.es/) complemented with information on atmosphere water content and near surface air temperature available from NWP fields.

The LSA SAF approach to estimate DSLF considers bulk parameterizations of the thermal radiative flux reaching the surface, $F^{\downarrow}$, emitted by an atmospheric layer with emissivity ε_{sky}, and temperature T_{sky}:

[Eq. 1] $$F^{\downarrow} = \sigma\, \varepsilon_{sky}\, T_{sky}^4$$

where σ is the Stefan-Boltzmann constant. The different parameterizations of ε_{sky}, and T_{sky} currently used in the operational system, or under study by the LSA SAF are systematized in Table 2.

Table 2 Terms of [Eq. 1] in the parameterizations considered by the LSA SAF. w = total column water vapour (mm); T_2 = 2m air temperature (K); Td_2 = 2m dew point (K); n = cloud fraction. Parameters α, β, γ, δ and m in the Prata_modified scheme are depend on the pixel cloud cover.

Scheme	ε_{sky}	T_{sky}	Applicability	Current Use
Prata (1996)	$1-\left(1+\frac{w}{10}\right)\exp\left(-\left(1.2+3\frac{w}{10}\right)^{1/2}\right)$	T_2	Clear sky	CLEAR SKY: EPS chain MSG chain – version 2.0 – 5.x
Dilley and O'Brien (1998)	$1-\exp(-1.66\tau)$ $\tau = 2.23-1.88(T_2/273)+0.74(w/25)^{1/2}$	T_2	Clear sky	CLEAR SKY: MSG chain –(until Sep 2006)
Josey et al. (2003)	1	$T_2 + 10.77n^2 + 2.34n - 18.44 + 0.84\,(Td_2 - T_2 + 4.01)$	All sky conditions	CLOUDY SKY: EPS chain MSG chain – version 0.1 – 5.x
Prata_Modified	$1-\left(1+\frac{w}{10}\right)\exp\left(-\left(\alpha+\beta\frac{w}{10}\right)^{m}\right)$	$T_2 + \gamma\,(T_2 - Td_2) + \delta$	All sky conditions	MSG chain – from version 6.0 onwards

3 Comparison of LSA SAF DSLF from SEVIRI with in-situ measurements

This section presents the validation results obtained from the comparison between LSA SAF DSLF and in situ measurements taken at the stations indicated in Figure 2, for the whole year of 2005. The DSLF values generated by the LSA SAF system in 2005 were obtained from the DSLF algorithm version **in use until July 2009**, based on the parameterization schemes by Prata (1996) for clear and Josey et al. (2003) for cloudy conditions (Table 2; Eq 1). The comparisons with in-situ data indicate an overall tendency for the LSA SAF to underestimate DSLF. The systematic

underestimation is particularly evident for the clear-sky DSLF (green dots in Figure 3), which tend to exhibit much less dispersion than the cloudy values. Although, the values of the clear sky bias vary considerably within the year (not shown in the current Validation Report), the annual values range from –12 Wm^{-2} (in Tamanrasset) to –19 Wm^{-2} (Carpentras).

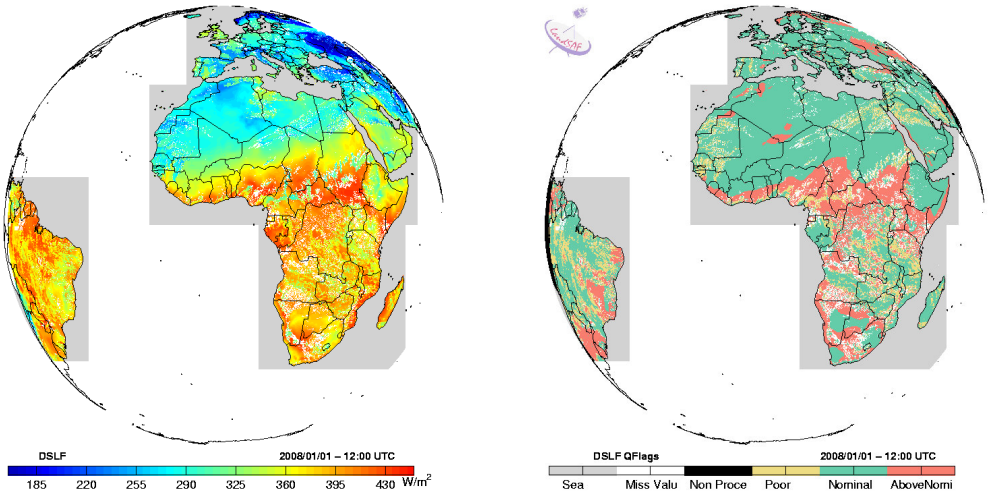

Figure 1 DLSF field (W/m^2; left panel) and respective quality flags (right panel) generated by the LSA SAF operational system for the 1st January 2008, at 12 UTC.

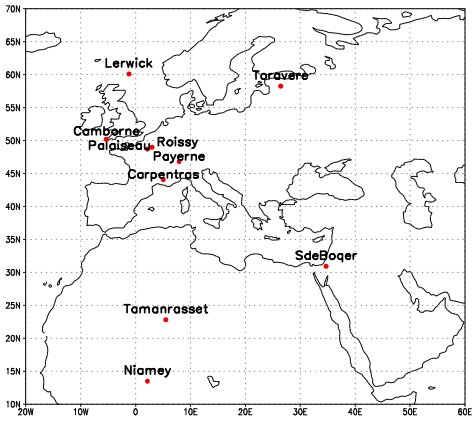

Figure 2 Location of stations with ground observations of downward longwave flux. Most stations are part of the Baseline Surface Radiation Network (BSRN), with the exceptions of Roissy and Niamey.

The range of bias obtained for cloudy and partially cloudy conditions is significantly higher among stations, and within the study period, for each station. The European sites present systematic differences mostly within –10 to –30 Wm^{-2} interval. The root mean square differences are generally higher, confirming the higher error dispersion of the estimated values, seen in Figure 3. Tamaransset, in Northern Africa, presents a much more pronounced underestimation of DSLF for the same conditions, with biases reaching -71 to –82 Wm^{-2} (not shown), for cloudy and partially cloudy conditions, respectively. The algorithm used until July 2009 for cloudy situations follows that developed by Josey et al. (2003), taking into account several campaigns, with a particular emphasis on measurements taken over the Atlantic ocean in mid-high latitudes. Although, it is difficult to take definite conclusion from the comparison with one single site, these results suggest the formulation should be revisited, particularly taking into account the large areas with dry warm atmosphere, which cover a large part of Meteosat disk.

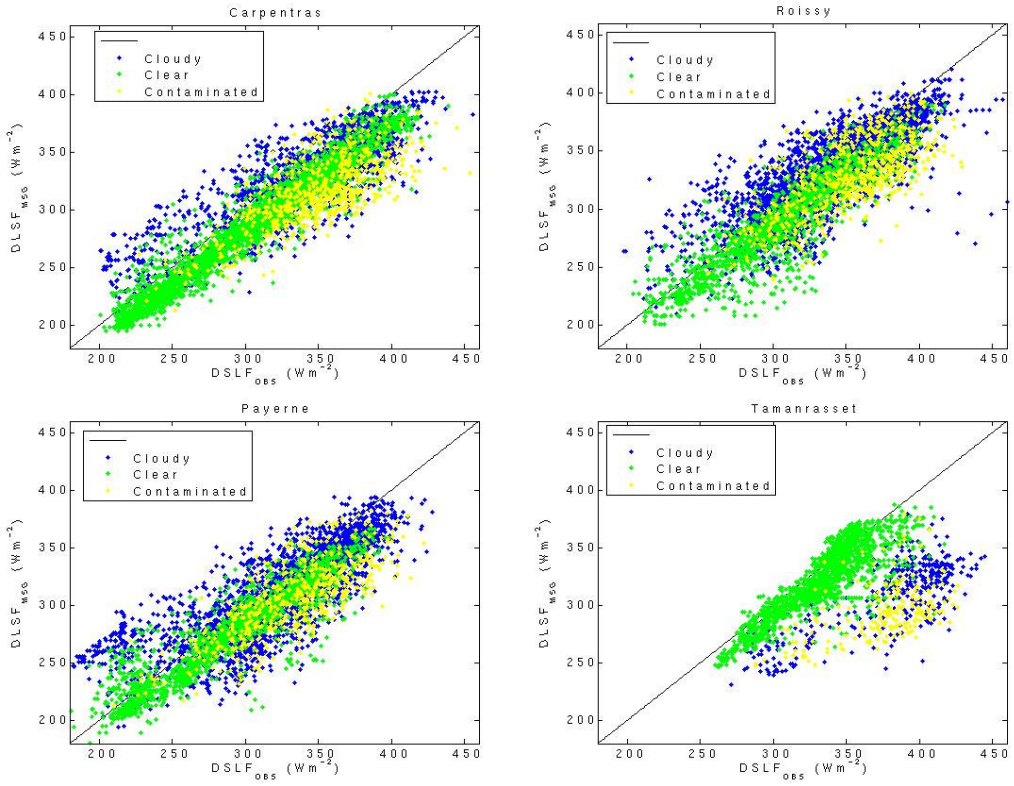

Figure 3 Scatterplots of Land SAF DSLF (y-axis) versus in-situ measurements (x-axis), for the January-December 2005 period, and for the locations indicated at the top of each panel,. The dots are coloured according to the pixel classification: green - clear-sky pixel; yellow – partially cloudy; and blue – cloudy pixel.

There are several sources of error for the (partially) cloud algorithms that explain the higher dispersion of the results, when compared with clear sky conditions. The adjustment for cloud type is performed indirectly through a cloudiness parameter, *n*, provided by the NWC SAF software: *n* is equal to 1 (lower than 1) for opaque (semi-transparent, i.e., thin cirrus) clouds. On the other hand, the algorithm developed by

Josey et al. (2003) made use of surface observations taken during oceanic campaigns, most of which over the Northern Atlantic. The atmospheric conditions for which the algorithm was trained are thus fairly limited, and leave out continental atmospheres characteristic of Tamanrasset.

Taking into account that user requirements regarding the accuracy of DSLF have been established in terms of relative error (Table 1), Table 3 shows the relative frequency of (2005) DSLF errors below 5%, within the 5-10% range, and above 10%. As expected, the partially cloudy situations present the worse performance, with frequencies of 40-to-90% of the estimated values not meeting the requirements. On the opposite side, clear sky estimation performs fairly well, despite the detected systematic errors.

Table 3 Percentage of cases with relative error of (2005) Meteosat-derived DSLF below 5%, within 5-to-10%, and above 10%.

	Carpentras			**Roissy**			**Payerne**			**Tamanrasset**		
	≤5%	**]5% 10%]**	**>10%**	**≤5%**	**]5% 10%]**	**>10%**	**≤5%**	**]5% 10%]**	**>10%**	**≤5%**	**]5% 10%]**	**>10%**
Clear	48.8	31.5	19.5	46.7	29.2	23.0	60.6	29.7	8.7	49.4	29.0	21.6
Partly	23.6	27.9	48.5	33.9	30.1	36.0	29.1	30.7	40.2	2.5	3.9	93.7
Cloudy	44.2	34.2	21.6	64.7	21.8	13.5	44.1	32.6	22.4	2.5	6.6	90.9

4 Assessment of Parameterization Schemes

The comparison against in situ measurements presented in the previous section suggests the 1st version of LSA SAF algorithm generally underestimated DSLF. This was particularly apparent for clear sky cases, with biases of the order of –10 to –20 Wm^{-2}. Cloudy pixels also exhibited negative biases (mostly within –10 Wm^{-2} to –30 Wm^{-2}, for European sites), but higher dispersion than in clear cases.

As a step forward to eliminate the detected biases, we have made an assessment of the different DSLF algorithms detailed in Table 2, valid for clear and cloudy conditions. The different schemes are compared with modelled data – MODTRAN and the ECMWF Radiative Transfer Model – and with in situ measurements (stations in Figure 2). The model data make use of the TIGR-like database (Chevalier et al., 2001), that samples temperature and humidity profiles within ECWMF re-analyses (ERA-40). This database presents a comprehensive and balanced set of atmospheric profiles, suitable for calibration/validation of radiative models/schemes. The aim of this exercise is (i) to rank the algorithms in terms of their accuracy; and (ii) to identify the main sources of errors, including cloud identification and classification. This study and the subsequent validation of DSLF algorithms against independent datasets supported the change of the method in the operational chain to the New_Parameterization or Prata_modified scheme in July 2009.

Figure 4 shows the scatterplots of bulk parameterization schemes against MODTRAN simulations of clear and cloudy cases, respectively. The new Prata_modified algorithm follows a generalization of the formulation proposed by Prata (1996), as indicated in Table 2; the respective coefficients were calibrated using the

MODTRAN simulations. The comparison between parameterization schemes and MODTRAN suggests a fairly agreement for all algorithms. In the case of cloudy conditions, the formulation developed by Josey et al. (2003) agrees well with MODTRAN for DSLF fluxes above ~300 Wm^{-2} only. It is worth noting that the method proposed by Josey et al. (2003) was calibrated using data collected during oceanic campaigns in the Northern Atlantic. The best fit between "Josey et al." parameterized values and MODTRAN simulations (Figure 4) is obtained for the range of values used for the algorithm calibration.

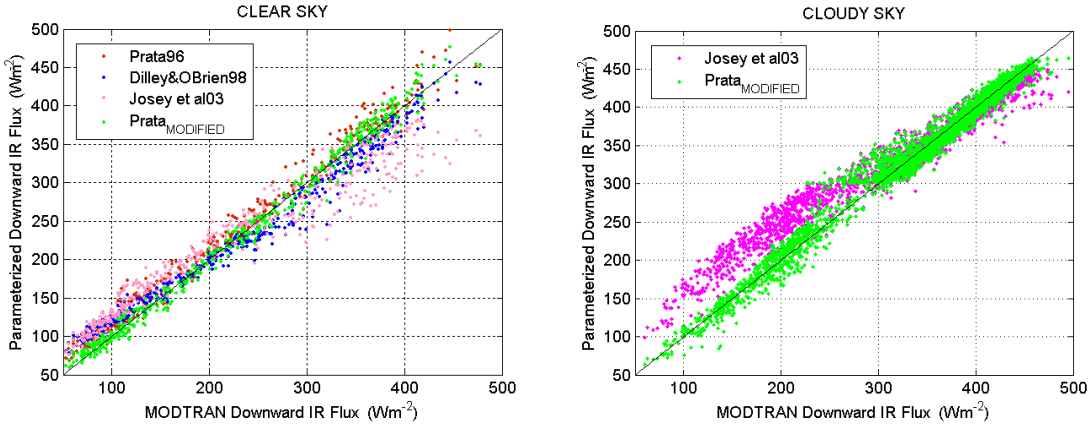

Figure 4 Scatterplots of DSLF values estimated using the bulk parameterization scheme indicated in the colour code versus MODTRAN simulations, for clear sky (left panel) and cloudy sky (right panel) conditions.

In the case of clear sky conditions, the respective scatterplot in Figure 4 suggests that the algorithm developed by Dilley and O'brien (1998) tends to overestimate (underestimate) MODTRAN simulations for low (high) flux values, while the algorithm developed by Prata (1996) tends to be slightly more stable. This is confirmed in Table 4, where the differences between MODTRAN and parameterizations are analysed in terms of water vapour content in the atmosphere. The algorithm proposed by Josey et al. (2003) is unable to model clear sky DSLF for (warm) atmospheres with large amount of water content. The results obtained for both clear and cloudy sky conditions suggest that this algorithm may have strong limitations in the simulation of DSLF over areas where atmospheric conditions are very different from those represented in the calibration dataset, namely (i) situations in extreme dry and cold continental areas; (ii) very warm and moist atmospheres, that occur in the tropics.

Table 4 Mean differences (bias) and root of mean square differences (RMSD) obtained between each parameterizations scheme and DSLF MODTRAN simulations of the TIGR-like database.

	Clear Sky		**Cloudy Sky**	
	Bias (Wm^{-2})	RMSD (Wm^{-2})	Bias (Wm^{-2})	RMSD (Wm^{-2})
Prata (1996)	8.2	16.9	-	-
Dilley and O'Brien (1998)	-4.2	21.2	-	-
Josey et al. (2003)	-1.7	35.7	5.9	28.28
Prata_modified	-0.1	10.6	+0.7	12.5

Table 4 summarises the statistics – bias and root mean square differences – between the different parameterization schemes and MODTRAN simulations. Not surprisingly, the Prata_modified algorithm presents the best results, since this algorithm was also calibrated with the same MODTRAN simulations. An independent assessment is presented next, where all formulations are validated against in situ data.

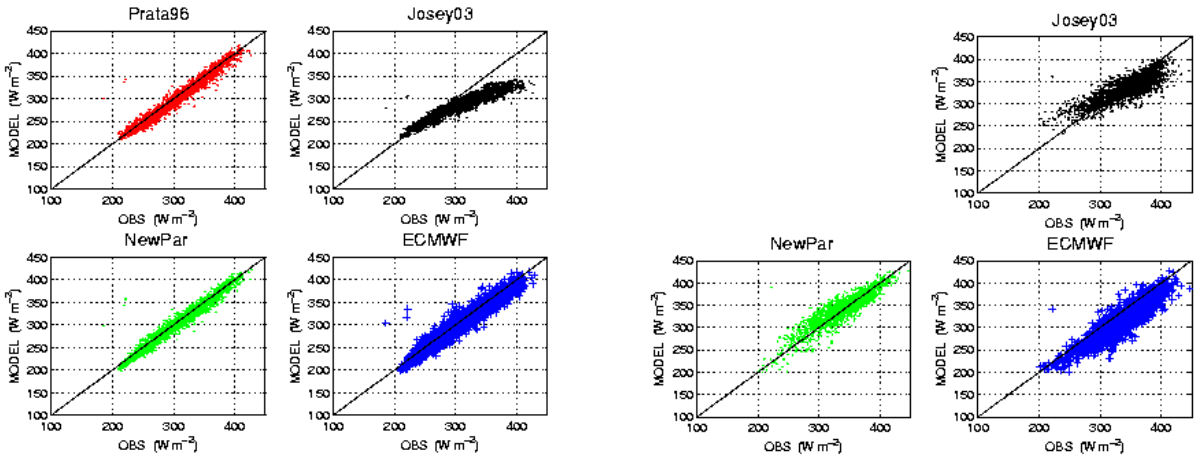

Figure 5 Scatterplots of DSLF (Wm^{-2}) obtained from different parameterization schemes (according to the title of each panel) against in situ measurements taken at Carpentras in France (horizontal axis). Blue crosses: ECMWF downward thermal fluxes at the surface, orographically corrected to the station height. Four left panels correspond to CLEAR SKY cases, while the right panels show the results for 3 models applicable to CLOUDY conditions.

DSLF obtained from SEVIRI/MSG data is then compared with ground observations, corresponding to 3-hourly averages (centred at 00, 03, … 18, 21 UTC). The algorithms used, as input, the NWP SAF Cloud mask and ECMWF forecasts of total column water vapour (TCWV), 2m dew point (Td2) and 2m-temperature (T2). The latter were orographically corrected to the station height, using a constant (moist air) lapse rate. The thermal infrared fluxes at the surface estimated by ECMWF model were also compared with in situ data, to be used as a benchmark. These values also correspond to 3-hourly averages centred at the observation time, and were corrected for the difference between model and station height, using a height gradient of 2.8 Wm^{-2}

$(100m)^{-1}$ (Wild et al., 1995; Morcrette, 2001). The comparison against in situ data is performed for a set of observations collected between May 2005 and December 2007, for the sites show in Figure 2; the total period of observations varies from station to station, but it corresponds to a minimum of 1 full year in all cases.

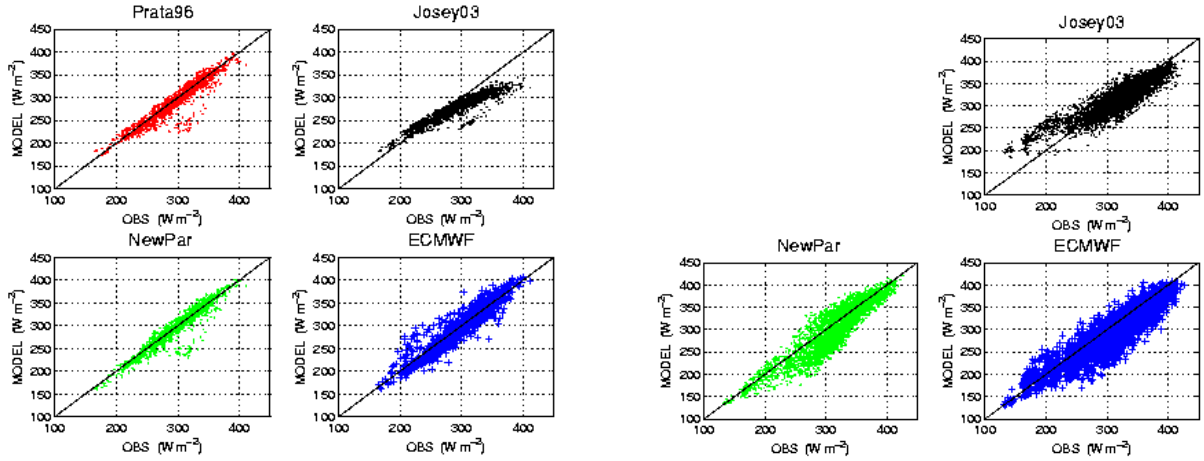

Figure 6 As in Figure 5, but for Toravere (Estonia).

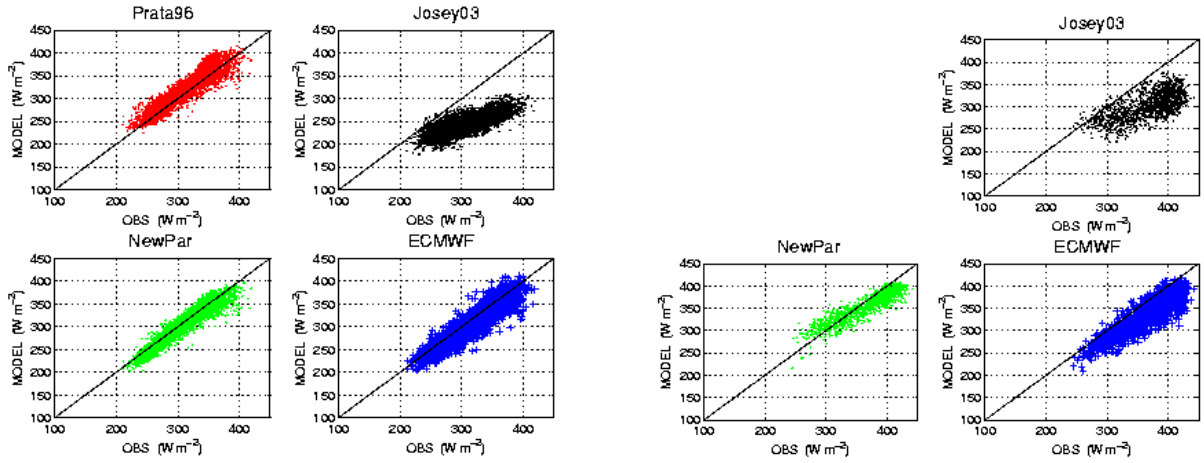

Figure 7 As in Figure 5, but for Tamanrasset (Sahara).

Figure 5, Figure 6, and Figure 7 present scatter plots of modelled DSLF values, using different formulations and ECMWF model, for 3 stations characteristic of middle latitudes, high latitudes, and arid regions, respectively. These diagrams generally confirm the results obtained with the comparison between parameterization schemes and MODTRAN simulations. Overall, the validation against in situ measurements indicates that the modified version of the algorithm initially proposed by Prata (1996),

performs better that the remaining formulations, for both clear and cloudy conditions, proving that the DSLF product can be significantly improved. The absolute biases of ~70-to-80 Wm^{-2} (obtained when the Josey03 formulation is applied) in Tamanrasset for cloudy cases were reduced to less than 10 Wm^{-2}.

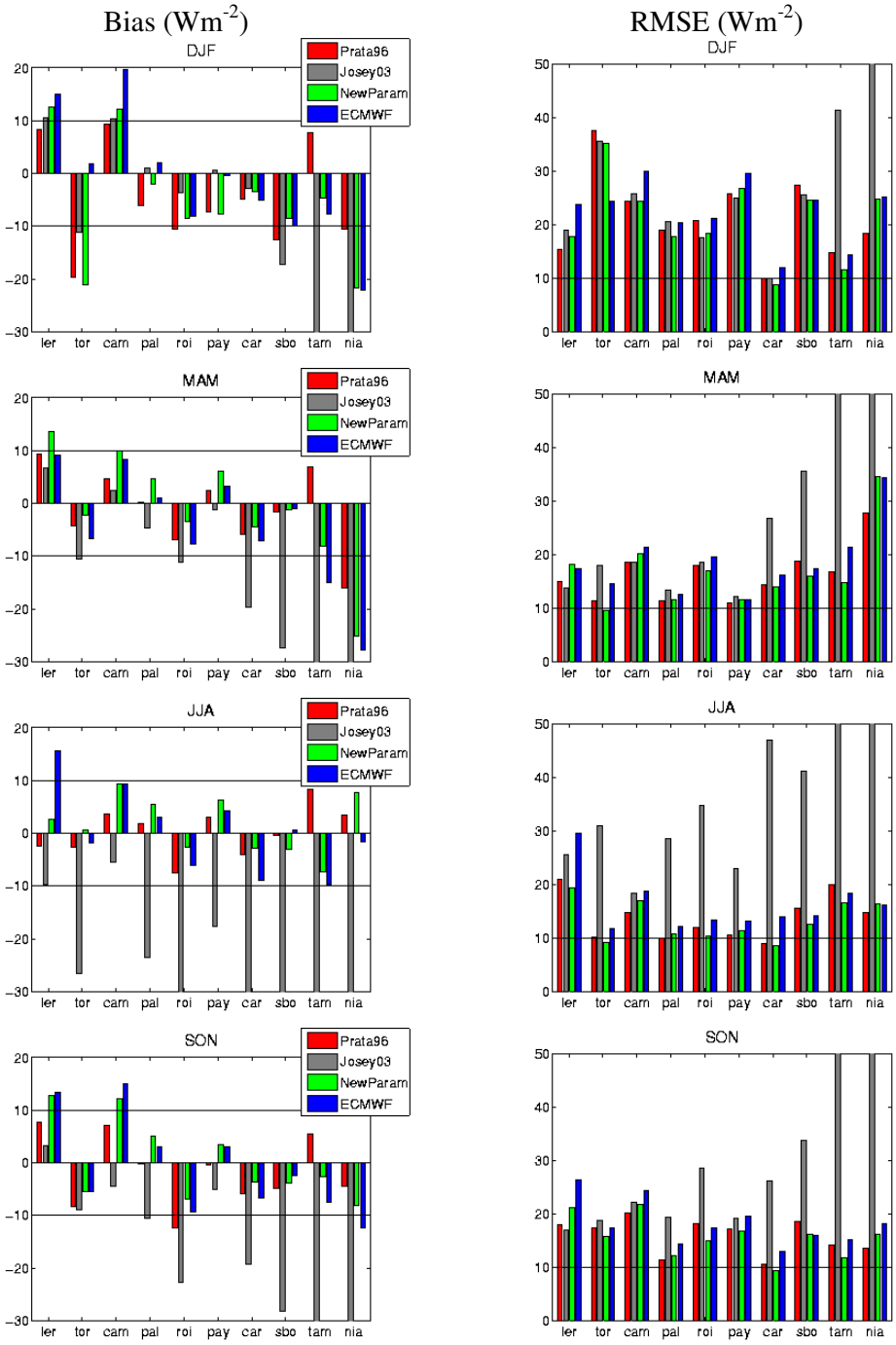

Figure 8 Seasonal bias (left column; Wm-2) root mean square differences (right column; Wm-2) between clear sky DSLF estimations and in situ observations, for the following stations: Lerwick, Toravere, Cambourne, Palaiseau, Roissy, Payerne, Carpentras, Sde Boqer, Tamanrasset, and Niamey. Statistics obtained for Prata96, Josey03, the new scheme, and for ECMWF correspond to red, grey, green, and blue bars, respectively. Please notice that there cases where Josey et al. (2003) bar is truncated, to ensure readability of the remaining elements in the respective diagrams.

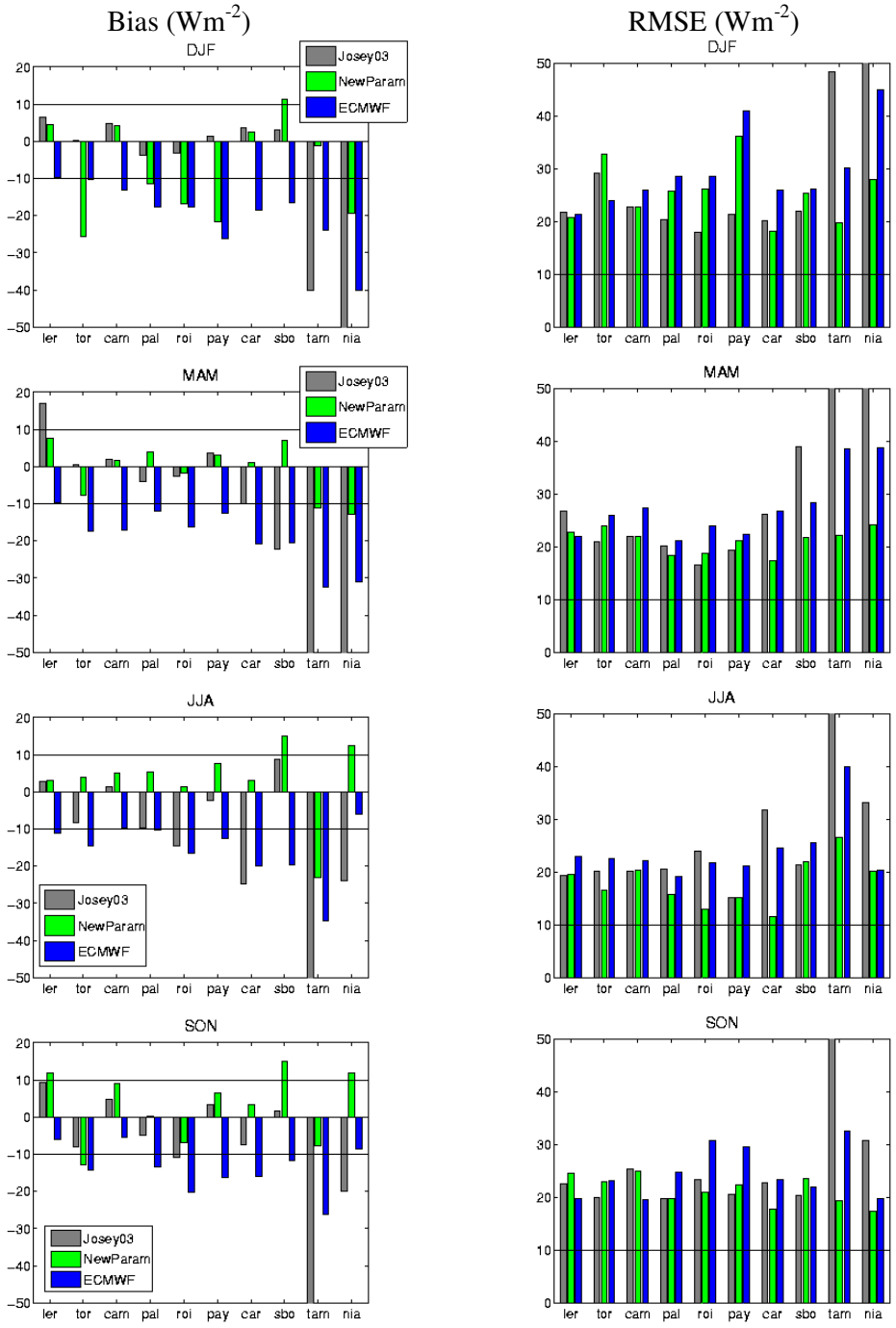

Figure 9 As in Figure 8, but for cloudy (overcast and partially cloudy) cases.

The scatter-plots in Figure 5, Figure 6, and Figure 7 show that dispersion around the 1:1 line is smaller for clear sky cases, than for cloudy conditions, when the thermal radiation reaching the surface depends on factors such as cloud base height and cloud microphysics. Under clear sky conditions, some of the stations show a few points with larger under-estimation of the observations (see Figure 6), which seem to correspond to undetected clouds. Toravere presents a set of such points clearly lying below the 1:1 line, most of which obtained during the winter months, when low solar zenith angles combined with high view angle makes the pixel classification more difficult.

The average differences and RMSE between DSLF estimations and in situ observations are show in Figure 8 and Figure 9, for DJF, MAM, JJA, and SON. Overall, the new parameterization scheme presents systematic errors below 10 Wm^{-2}, with the exception of the cases discussed below. The new scheme also tends to perform better than ECMWF simulations, suggesting that despite its simplicity it partially corrects for deficiencies in ECMWF cloud modelling (e.g., Crewel et al., 2002; Meetschen et al., 2004), benefiting as well of the finer spatial representation of the remote sensing cloud mask. The results obtained using the scheme developed by Josey et al. (2003) are the most variable: DSLF estimations are comparable with those obtained from other schemes in middle-to-high latitude stations, but present strong negative bias during the warm season in Europe, and during all year round in the most southern stations (Sde Boquer in Israel, Tamanrasset in Algeria and Niamey in Niger). The modified version of the Prata formulation for cloudy conditions outcomes Josey03 simulations for most stations. For clear sky conditions, the scores obtained by the original and modified version of Prata's algorithm are fairly similar.

The new parameterization scheme exhibits poorer performances for Toravere during the winter months, where it underestimates local observations by over 20 Wm^{-2}, in both clear and cloudy sky conditions. The clear sky results may be partially explained by an under-classification of cloudy scenes. The cloudy sky scores are not fully understood. Niamey, particularly during DJF and MAM, is another critical site, where the modified Prata formulation underestimates local observations of clear and cloudy fluxes. The Niamey region was characterized by relatively high aerosol loads, and also suffered severe dust storms in March (Slingo et al., 2006). The parameterization formulations analysed here, and the ECMWF model, were clearly unable to simulate the atmospheric downward fluxes in such extreme conditions.

5 Daily DSLF from SEVIRI/Meteosat (DIDSLF)

The daily DSLF (DIDSLF) corresponds to the accumulation (0 – to – 24 UTC) of instantaneous SEVIRI/Meteosat DSLF computed every 30-min. The fields are made available along with the percentage of missing time-slots through the accumulation period, estimated on a pixel-by-pixel basis.

This section presents the most recent validation results obtained for the LSA SAF DIDSLF product. The fields produced for the period between August and December 2009 are analysed for consistency. Generated fields and global statistics are compared to ECMWF forecasts of daily accumulated downward thermal fluxes The

DIDSLF SEVIRI data are also compared with the available ground observations from the BSRN database for the 2010 period.

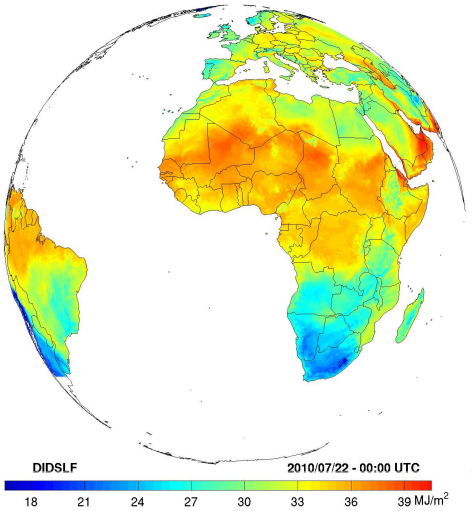

Figure 10 DIDSLF field (MJ/m^2) generated by the LSASAF operational system for the 22 nd July 2010.

5.1 Overall assessment of DIDSLF

This section presents an overall assessment of the DIDSLF. For an easier interpretation of the results, we opted to convert the original units of daily fluxes (J m^{-2}) to [W m^{-2}], dividing DIDSLF by (24 × 3600 s).

The period under analysis ranges from August to December 2009. August 2009 coincides roughly with the migration of the new parameterization scheme (Prata_modified) from the parallel to the operational LSA SAF processing chain. The overall assessment presented in this section is performed by (i) checking the temporal evolution of the data, (ii) verifying the frequency of missing 30-minute slots and impacts on the daily product, and (iii) comparing with ECMWF forecasts (thermal downward fluxes forecasts accumulated through steps 12 – to – 36 hours).

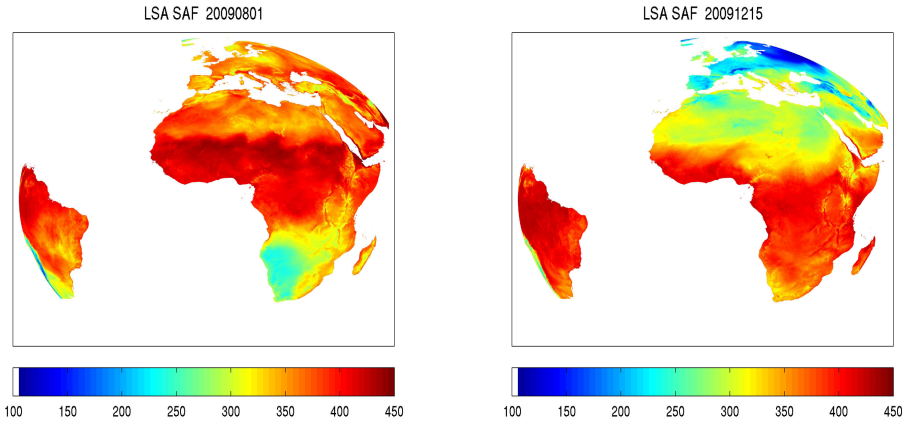

Figure 11 – Daily DSLF product obtained from SEVIRI (DIDSLF, product ID LSA-12) obtained for 1 August 2009 and 15 December 2009. The daily product (J m^{-2}), corresponding to the accumulation of 30-minute instantaneous DSLF fields derived from SEVIRI, was divided by (24 × 3600 s) and therefore converted to [W m^{-2}].

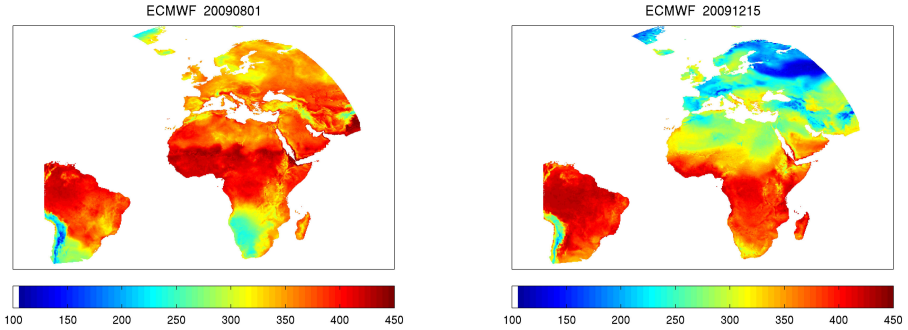

Figure 12 As in Figure 11, but for daily thermal flux (also converted to W m^{-2}) obtained from ECMWF forecasts. Values over sea were masked out to make the comparison with LSA SAF products easier.

As an example, Figure 11 shows estimated daily DSLF for two days (1 August 2009 and 15 December 2009), for which the fraction of missing time-slots was 2% or less. The latter correspond to the relative number of 30-minute DSLF_SEVIRI values not available in the respective 0 – 24 UTC period. The daily DSLF values and patterns are in accordance to the equivalent fields obtained from ECMWF forecasts for the same days (Figure 12). Although the fields in Figure 11 and Figure 12 are represented in different projections (original SEVIRI geostationary projection and a regular 0.25ºx0.25º, respectively), they show values within the same range and common features such as: (i) area of minimum flux values in Southern Africa in August; (ii) the patterns over the Sahara in December; (iii) the pronounced maxima over the Sahel in August. Figure 13 shows the distribution of the differences "SAF – ECMWF" daily DSLF, for the whole study period, after SAF fields were interpolated to ECMWF regular grid. Apart from a reduced number of outliers, most discrepancies are within 20W m^{-2}, over the Euro, NAfr and SAfr areas. For SAme, however, differences are generally within 20 and 35 W m^{-2}. As will be shown below, such positive bias seems to be enhanced over the Andes, where the LSA SAF product is influenced by a better representation of local topography when compared with ECMWF model.

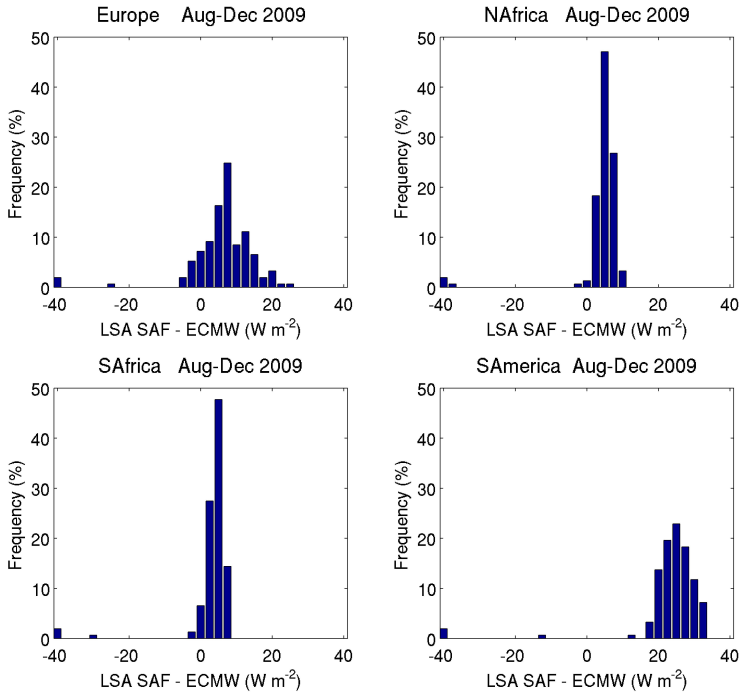

Figure 13 Distribution of differences "SAF – ECMWF" daily DSLF, obtained for the August 2009 to December 2009 period, represented for each of the LSA SAF geographical areas.

Systematic errors in instantaneous SEVIRI DSLF will be propagated to the daily accumulated values, while random errors tend to be smoothed when temporal integrations are performed. Therefore, the major source of errors in the daily DSLF

product beyond propagation of DSLF_SEVIRI uncertainties relies on the existence of missing data within the daily integration period. Next we assess how such missing data impacts on the output.

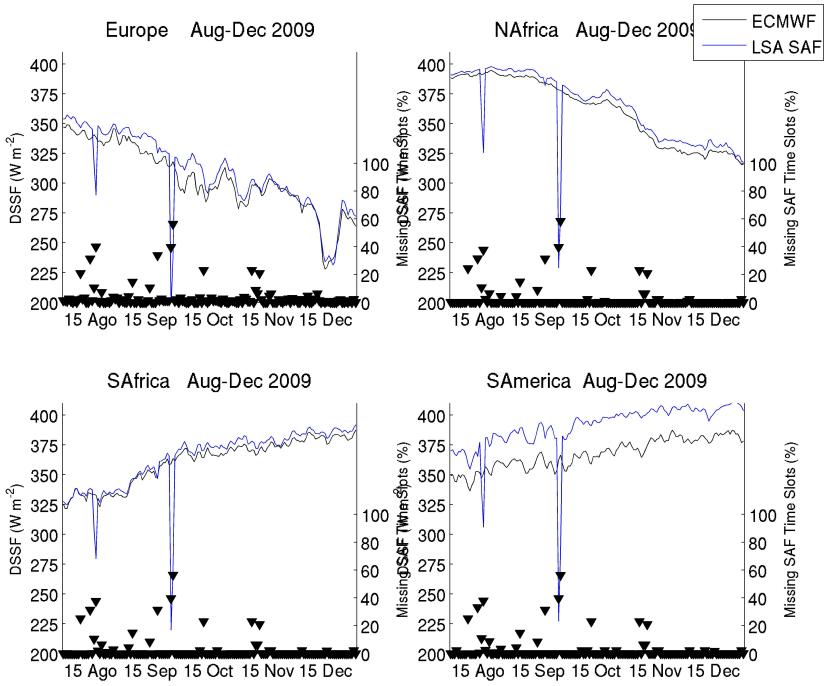

Figure 14 Time-series of SAF daily DSLF product (blue line) and of ECMWF downward thermal flux (black line), both averaged over each LSA SAF geographical area, for the August – December 2009 period. The triangles represent the percentage of missing LSA SAF time-slots per day, also averaged over each area (right axis).

The time-series of daily DSLF, averaged over each LSA SAF area (Figure 14) follow quite closely the equivalent ECMWF curve. However, the LSA SAF seems to estimate systematically higher fluxes than ECMWF, by values ranging from about 5 Wm^{-2} (NAfr and SAfr), 10 Wm^{-2} (Euro) and about 25 Wm^{-2} (SAme). Such discrepancies are consistent with the results discussed in section 4, where comparisons with in situ data suggest more pronounced negative biases in JJA and SON, for ECMWF when compared to the LSA SAF (particularly Figure 9)

(Fig) also puts into evidence the negative impact of missing data on the quality of daily DSLF: the outliers, generally associated to anomalously low flux estimations, correspond to high percentage of missing slots, typically above 40%. Missing slots may occur because of momentaneous stops of the operational chain, or missing input data (including complete files or image segments). Given the importance of data availability, the percentage of missing data, estimated on a pixel by pixel basis is also provided to users.

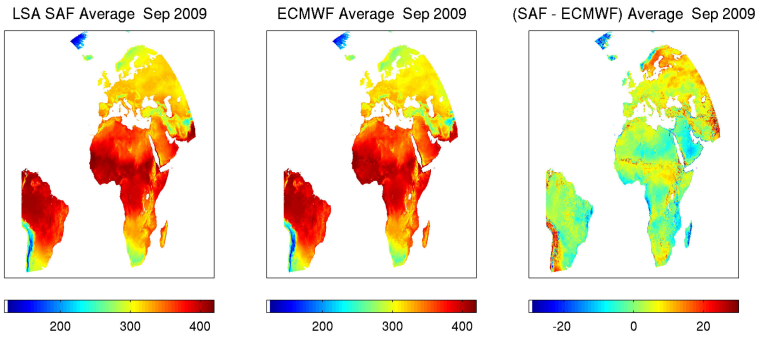

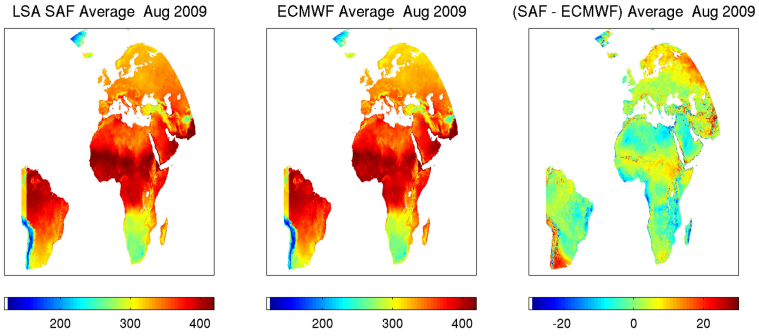

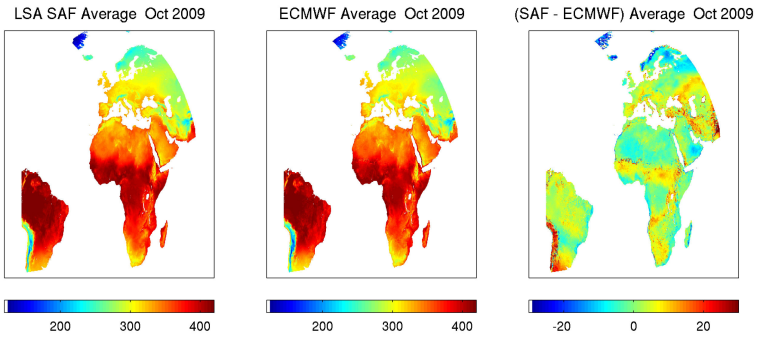

(Figure 15 – cont.)

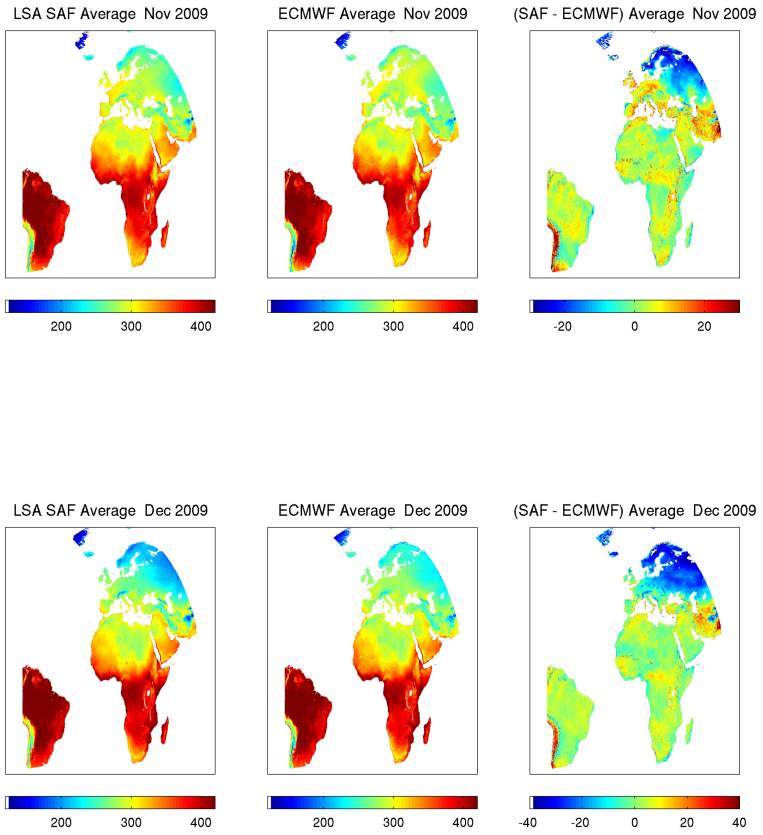

Figure 15 August 2009 monthly averaged fields of (left panel) LSA SAF daily DSLF (Wm^{-2}) re-projected on a 0.25º x 0.25º regular grid; (middle panel) ECMWF daily fluxes (Wm^{-2}); and (right panel) respective difference ($W\ m^{-2}$). Only pixels and days with 10% missing slots during the 0 - 24 UTC period, or less, were taken into account for the statistics.

Figure 15 shows monthly averages of LSA SAF and ECMWF daily fluxes, and the respective differences. First, LSA SAF daily DSLF fields were re-projected to ECMWF regular grid, by averaging all pixels that fall within a 0.25º x 0.25º grid box. Then, both the LSA SAF and ECMWF monthly means were estimated considering days with the percentage of missing LSA SAF DSLF_SEVIRI equal to 10% or less. Again, the range of values and main features are present in LSA SAF and ECMWF monthly fields. Systematic differences between flux estimations are generally less than 10 $W\ m^{-2}$, with higher LSA SAF fluxes with respect to ECMWF estimated over the Sahel, part of the Sahara (in accordance with the results shown in Figure 8 and Figure 9 for Tamanrasset) or South America. It is worth noticing that over the North-eastern part of

the disk, "LSA SAF minus ECMWF" differences seem to shift from positive values in summer months to strongly negative ones in November and December. The latter may be associated to an underestimation/overestimation of cloudy conditions by the LSA SAF/ECMWF, as well as to unresolved problems with the DSLF parameterization under very cold conditions (see results for Toravere in winter, Figure 8 and Figure 9).

5.2 Comparison against in situ observations

The comparison was performed for 6 stations from the BSRN database. The stations cover different geographical areas (indicated in Table 5) under a high range of meteorological conditions. The considered stations include 2 high latitude sites, Toravere, located in northeastern Europe, and Cabauw, a coastal station in the Netherlands. The considered sites also include a middle latitude station, Carpentras located in southern France, and 2 semi-arid/desert sites - Tamanrraset, located at a high plateau in Algeria, and Sede Boqer in Israel. Finally a station located in Canarias Islands with high elevation gradient, Izaña, is also used. In order to correct the differences in height between the in situ stations and the LSASAF considered elevations the DIDSLF product was adjusted using a height gradient of 2.8Wm^{-2}/100m following the approach of Wild et al. (1995). The comparison period was chosen as the maximum available time-series for each station, ranging from January to May, for the shortest time series available, in Tamanrasset and from January to September for the longest time-series in Izaña and Toravere.

Table 5 Stations with in situ measurements of downward long-wave radiation used for the validation of DIDSSF.

Station	Latitude & Longitude	Altitude (m)
Toravere	58.25°N; 26.46°E	30
Carpentras	44.05°N; 5.03°E	100
Sede Boqer	30.91°N; 34.78°E	500
Izaña	8.30°N; 16.42°W	2367
Tamanrasset	22.78°N; 5.51°E	1385

Taking into account that user requirements regarding the accuracy of DIDSLF established in terms of relative error (Table 1), Table 6 shows the DIDSLF frequency distribution of optimal values (errors below 5%), target values (errors within the 5-10% range), threshold values (errors within the 10-20% range) and large error values (errors above 20%).

In general errors are below 5% or within 5-10% range for sites located in LSA SAF area Euro. For Carpentras the product presents the best performance: for the whole period under consideration, errors are below 5% for more than 70% of the cases. An exception to this pattern is found in Toravere (a northeastern site with high viewing

angles) during winter months, where the majority of errors are within the 10-20% range from January to March. For all stations analyzed here, the DIDSLF performance is worse for winter months.

Table 6 Percentage of cases with relative error of SEVIRI-derived DIDSLF below 5%, within 5-to-10%, within 10-to-20% and above 20%, for Cabauw, Carpentras and Toravere.

	CABAUW				CARPENTRAS				TORAVERE			
	≤5%	]5, 10]%	]10, 20]%	>20%	≤5%	]5, 10]%	]10, 20]%	>20%	≤5%	]5, 10]%	]10, 20]%	>20%
January	25.8	45.2	29.0	0.0	70.0	30.0	0.0	0.0	0.0	3.2	64.5	32.3
February	28.6	53.6	14.3	3.6	85.7	14.3	0.0	0.0	0.0	10.7	64.3	25.0
March	67.7	29.0	3.2	0.0	83.9	16.1	0.0	0.0	9.7	35.5	38.7	16.1
April	90.0	3.3	0.0	6.7	100.0	0.0	0.0	0.0	73.3	23.3	3.3	0.0
May	96.8	3.2	0.0	0.0	100.0	0.0	0.0	0.0	77.4	22.6	0.0	0.0
June	93.3	0.0	3.3	3.3	93.3	0.0	3.3	3.3	70.0	23.3	3.3	3.3
July	100.0	0.0	0.0	0.0	100.0	0.0	0.0	0.0	96.8	3.2	0.0	0.0
August					100.0	0.0	0.0	0.0	96.8	3.2	0.0	0.0
September									80.0	20.0	0.0	0.0

Figure 16 to Figure 18 presents the time series of DIDSLF product and in situ measurements within the LSASAF Euro area. The time-series of DIDSLF follows quite closely the respective in situ value. However for sites with higher satellite viewing angles, and during winter months, the LSA SAF product seems to underestimate the in situ observations by values ranging from about 2.0 MJm^{-2}, in Cabauw, to 4.0 MJm^{-2}, in Toravere, and RMSD ranging from 2.3 MJm^{-2} for Cabauw, and 4.3 MJm^{-2} for Toravere (Table 7, comparisons with large number of missing values for measures and/or DIDSLF were not considered). On the other hand the middle latitude station, Carpentras, performs quite well even in winter months with absolute bias lower than to 0.79 MJm^{-2} and RMSD of the order of 1.13 MJm^{-2} or less.

A closer inspection of the time-series reveals that higher values of bias and RMSD are, as expected, related to missing values of DIDSLF product and/or missing in situ observations. Large errors are also present in high latitudes during winter months, in line with the results obtained for the instantaneous flux values (DSLF) discussed in section 4 and in Trigo et al. (2010).

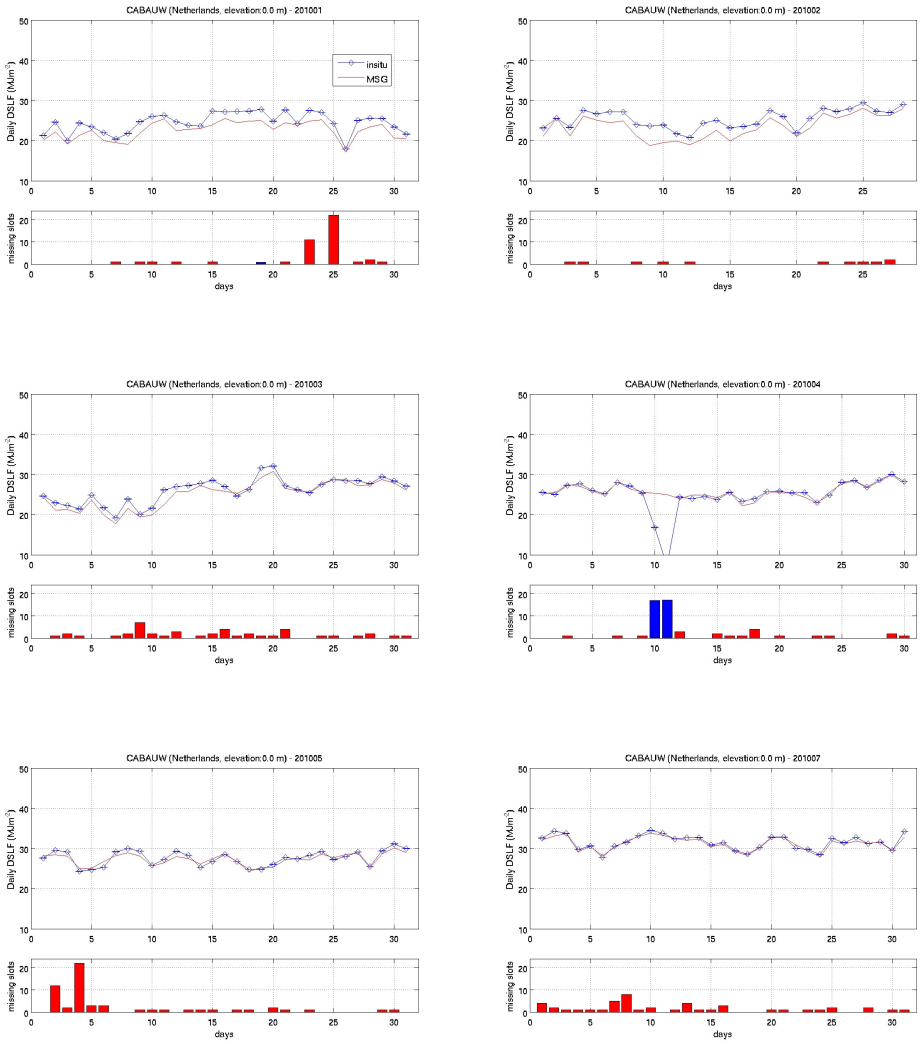

Figure 16 Upper panels: time-series of daily in situ observations at Cabauw (blue line) and DIDSLF product (red line), for the month indicated in top of each diagram; Lower panel: percentage of missing values of in situ instantaneous (1-minute) observations (blue bar) and percentage of missing values of DSLF (i.e., 30-minute instantaneous fluxes) (red bar), per day.

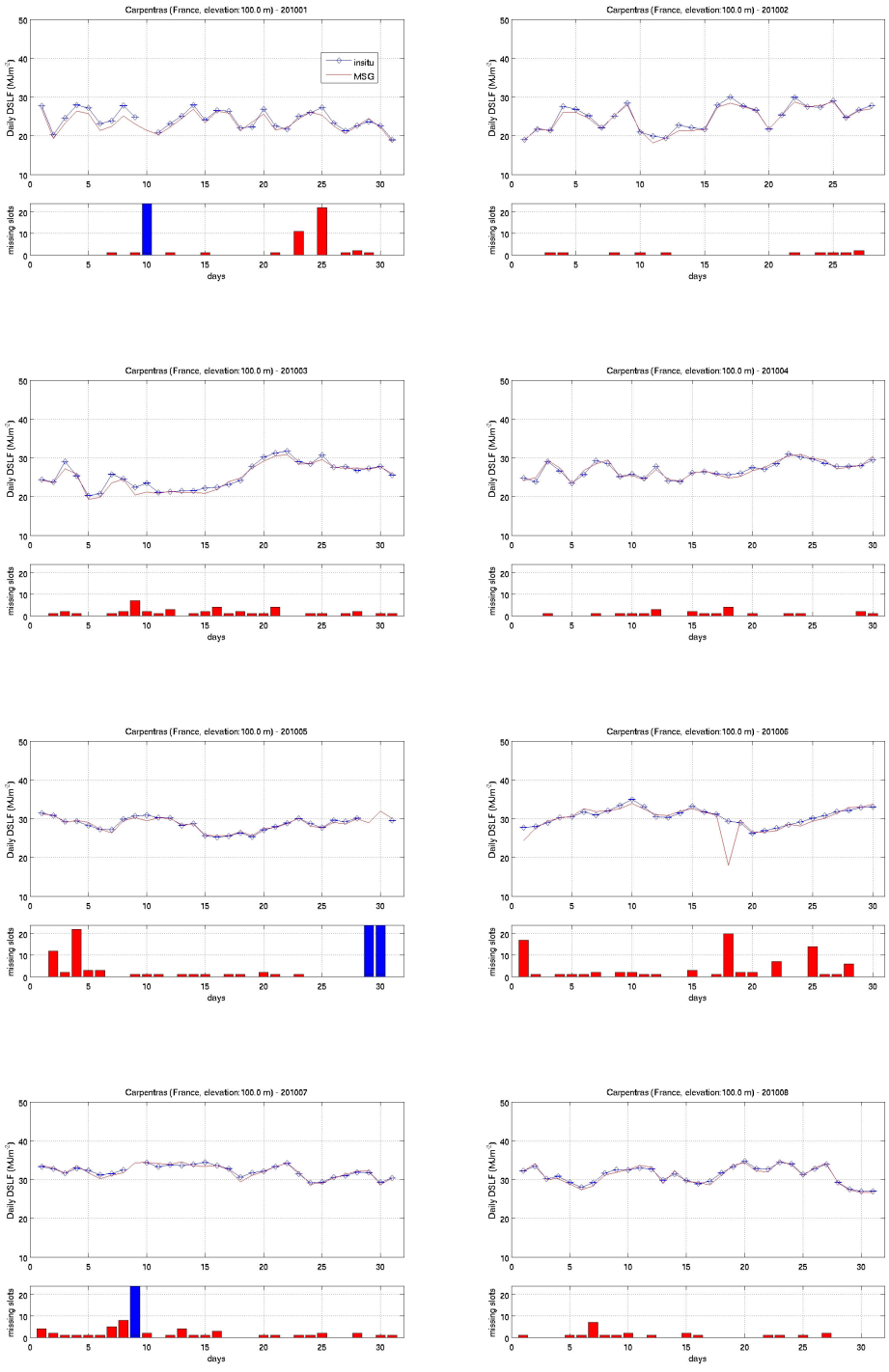

Figure 17 As
Figure 16 but for Carpentras.

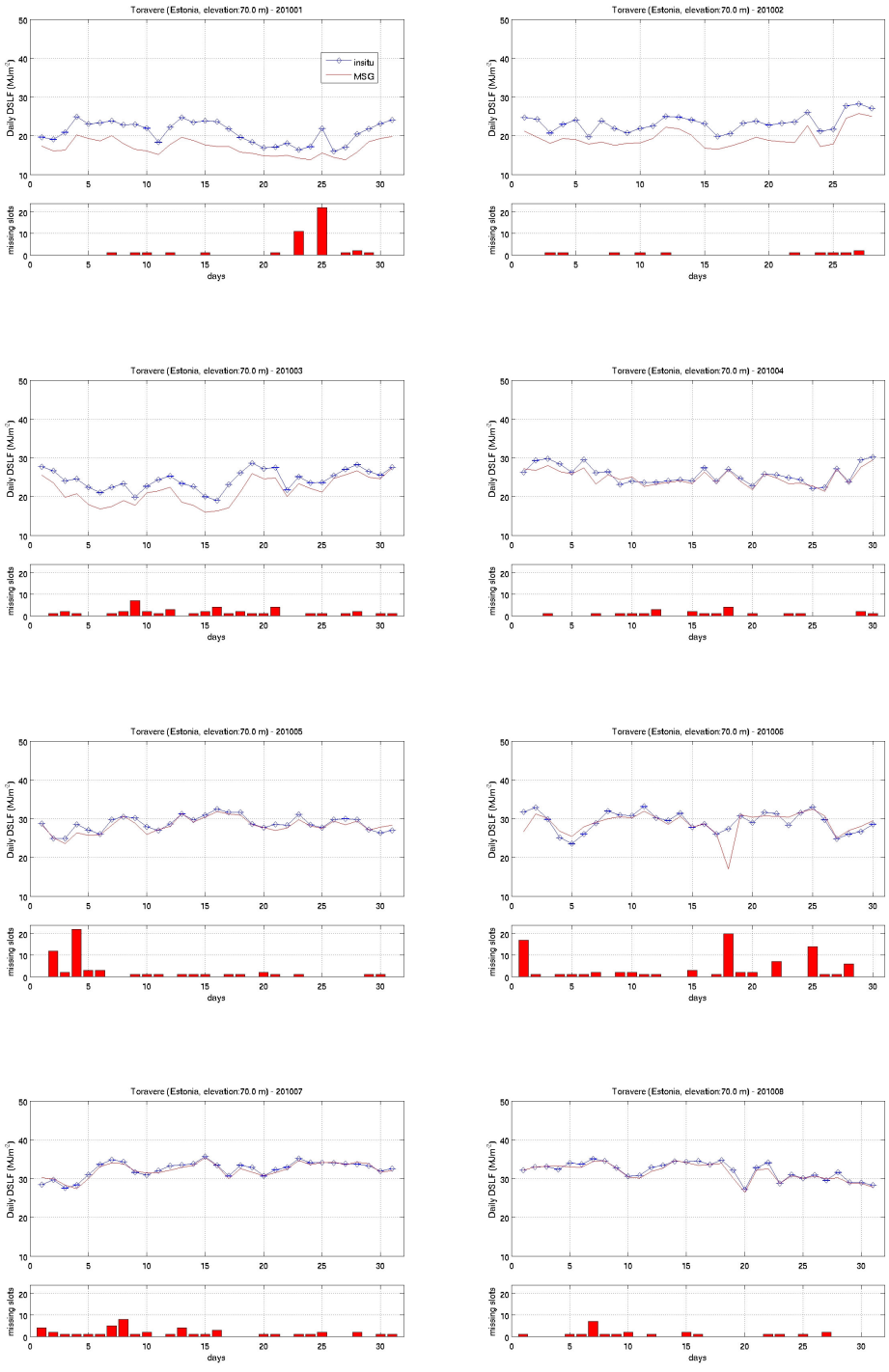

Y

Figure 18 As
Figure 16 but for Toravere.

Table 7 summarizes the statistics- mean, bias and root mean square differences – for each station within LSA SAF area Euro.

Table 7 DIDSLF: mean in situ observations, mean SEVIRI–derived values, bias and root mean square differences (RMSD), for Cabauw, Carpentras and Toravere. * Measured values in Cabauw during April should be regarded carefully due to the large number of missing information. For all stations, June should be regarded carefully due to the large number of missing DIDSLF values.

	CABAUW				CARPENTRAS				TORAVERE			
	Mean Isitu MJm^{-2}	Mean SEVIRI MJ m^{-2}	Bias insitu-SEVIRI MJ m^{-2}	RMSD insitu-SEVIRI MJ m^{-2}	Mean Isitu MJm^{-2}	Mean SEVIRI MJ m^{-2}	Bias insitu-SEVIRI MJ m^{-2}	RMSD insitu-SEVIRI MJ m^{-2}	Mean Isitu MJm^{-2}	Mean SEVIRI MJ m^{-2}	Bias insitu-SEVIRI MJ m^{-2}	RMSD insitu-SEVIRI MJ m^{-2}
January	24	23	1.93	2.11	24	23	0.79	1.13	21	17	4.04	4.25
February	25	23	2.01	2.27	25	24	0.42	0.72	23	20	3.77	3.91
March	26	25	0.97	1.35	25	25	0.52	0.95	24	21	2.91	3.25
April	25	26	-0.72*	3.64*	27	27	-0.04	0.61	26	25	0.75	1.23
May	28	27	0.30	0.79	29	29	0.10	0.46	29	28	0.55	0.98
June	29	28	1.01	2.62	31	30	0.54	2.25	29	29	0.37	2.35
July	32	31	0.32	0.54	32	32	0.11	0.54	32	32	0.27	0.69
August					31	31	0.17	0.52	32	32	0.44	0.75
September									29	29	0.69	1.09

The performance of DIDSLF product in BSRN stations located in LSASAF NAfr area was also assessed. This set of sites present very different conditions from those used for the Euro area. In fact, Sede Boqer and Tamanrasset are located in arid regions and the latter is on a plateau at 1385m. A particular case is the Izaña site that is located in an island with large elevation gradients.

Table 8 shows the DIDSLF frequency distribution of errors. In general errors are below the 10% range. For Sede Boqer the majority of product values (over 60%) present errors below 5%, for the whole period considered. The product performance in Tamanrasset is mostly within the target to optimal range. A different behaviour is found for Izaña where the majority of values can be considered within the target to threshold interval, except for the July to September period when these values are mainly optimal. In Izaña, unlike the other two sites a significant percentage of errors are beyond threshold the accuracy of 20%.

Table 8 As Table 6 but for Sede Boqer, Izaña and Tamanrasset stations

	SEDE BOQER				IZAÑA				TAMANRASSET			
	≤5%	]5, 10]%	]10, 20]%	>20%	≤5%	]5, 10]%	]10, 20]%	>20%	≤5%	]5, 10]%	]10, 20]%	>20%
January	64.5	29.0	6.5	0.0	19.4	25.8	45.2	9.7	29.0	51.6	19.4	0.0
February	60.7	28.6	10.7	0.0	18.5	25.9	48.1	7.4	57.1	42.9	0.0	0.0
March	74.2	25.8	0.0	0.0	19.4	25.8	41.9	12.9	19.4	71.0	9.7	0.0
April	90.0	10.0	0.0	0.0	33.3	40.0	16.7	10.0	20.0	80.0	0.0	0.0
May	87.1	12.9	0.0	0.0	25.8	29.0	32.3	12.9	25.8	58.1	16.1	0.0
June	73.3	20.0	3.3	3.3	36.7	20.0	30.0	13.3				
July					61.3	29.0	9.7	0.0				
August					83.3	13.3	3.3	0.0				
September					56.7	26.7	13.3	3.3				

As for the Euro stations the DIDSLF product, in Sede Boqer and Tamanrasset, tends to underestimate observations with positive bias values ranging from 0.58 to 2.22 MJm^{-2} and RMSD from 1.24 to 2.43 MJm^{-2} (Table 9). The worse values of the statistics are mainly associated with missing values of DIDSLF product in May and June (Figure 19 and Figure 20).

For Izaña the conclusions are quite different. As mentioned before, errors are higher than for the other 2 stations except in the July-to-September period. Moreover, visual inspection of the time series for this station (Figure 21) shows that the product clearly overestimates observations, except for the above mentioned period where the overestimation is less evident. DIDSLF bias at Izaña is negative and ranges from -2.28 MJm^{-2} in March to -0.06 MJm^{-2}, in August. High values of RMSD (above 2.4MJm^{-2}) are also found for this site, except for the July-September period (Table 9).

The mean meteorological conditions for August and March at Izaña are plotted in Figure 22. In July-September Izaña is under the influence of the semi-permanent high pressure belt located at its northern position, and the eastern flux from the Sahara, which brings warm deep dry air. As a consequence, the region and the station location are essentially under clear sky conditions, at this time of the year. From January to April, the region is under the influence of more variable flux and the eastern circulation is not so well defined. The island is often covered with stratocumulus, however, since the station is at very high altitude (about 2373 m) it is located above the top of the boundary layer (as can be confirmed by T-skew diagrams for Tenerife, not shown in the current report). Therefore, while the station records downward fluxes under clear sky, its surroundings at lower parts of the island are covered by stratocumulus, leading to satellite classifications of cloudy or partly cloudy. Under such conditions, more likely to occur from January to May, the station measurements will not be representative of the pixel scale. Accordingly, the number of pixels classified as cloudy or partly cloudy in March for Izaña site reaches 43.2% of retrievals, while in August this number is only 5.2% (Table 10)

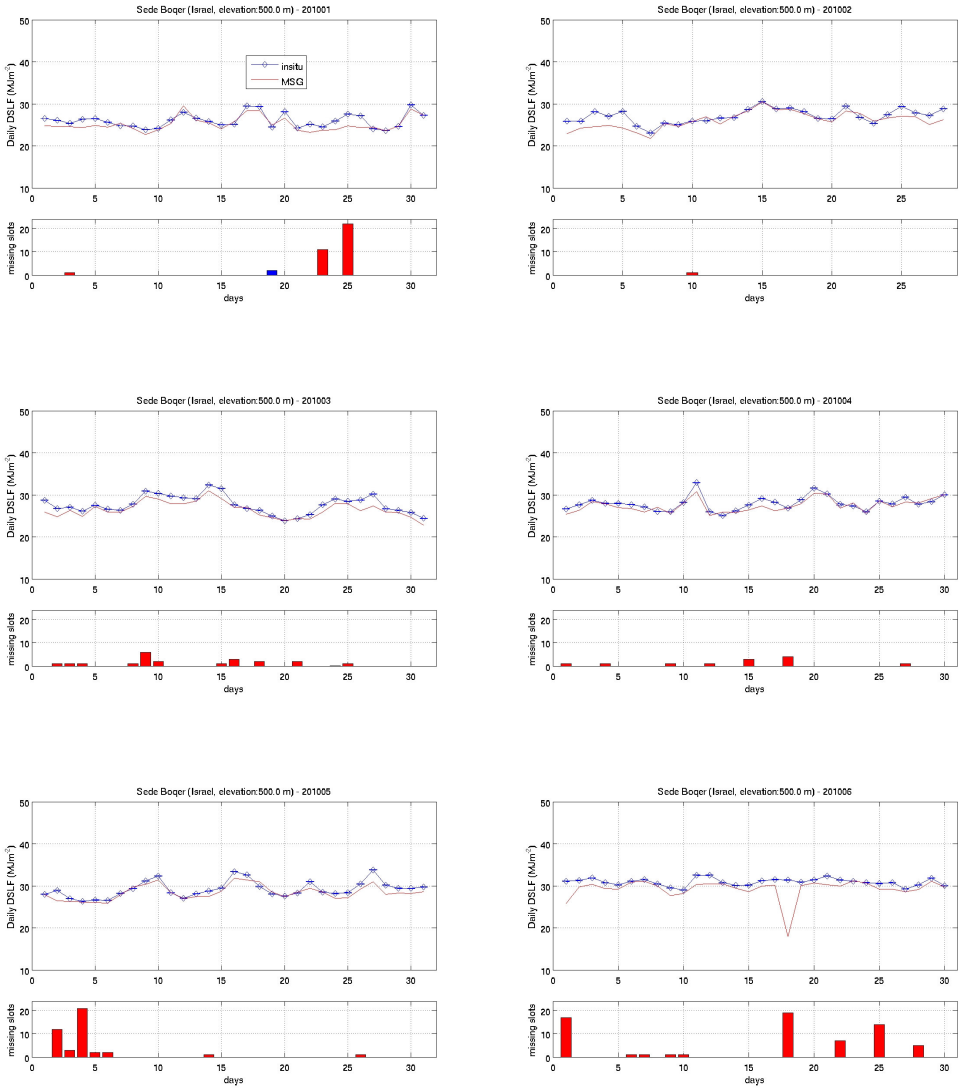

Figure 19 As in
Figure 16 but for Sede Boqer.

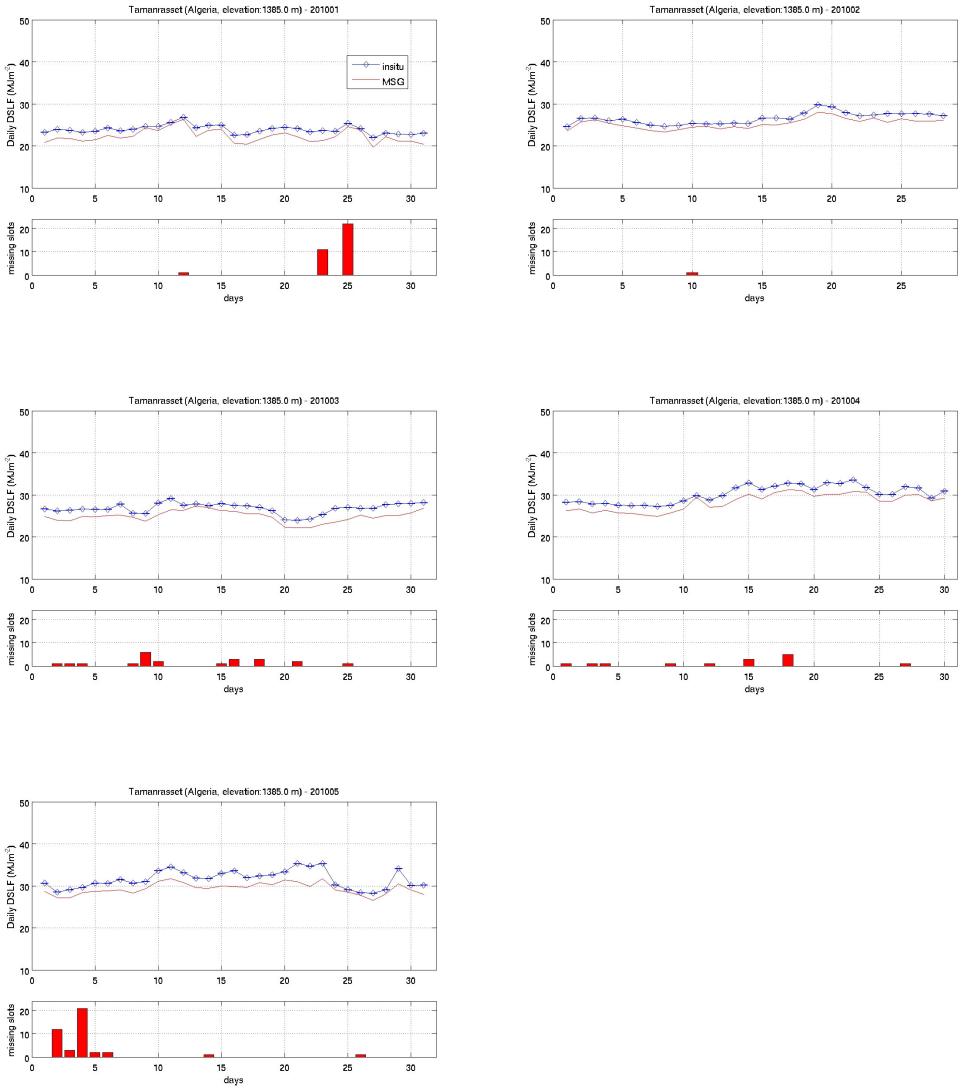

Figure 20 As in
Figure 16 but for Tamanrasset

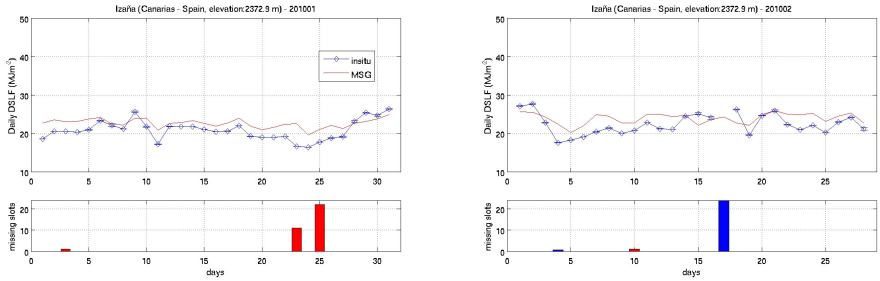
Izaña (Canarias - Spain, elevation:2372.9 m) - 201001
insitu
MSG
Daily DSLF (MJm-2)
missing slots
days

Izaña (Canarias - Spain, elevation:2372.9 m) - 201002
Daily DSLF (MJm-2)
missing slots
days

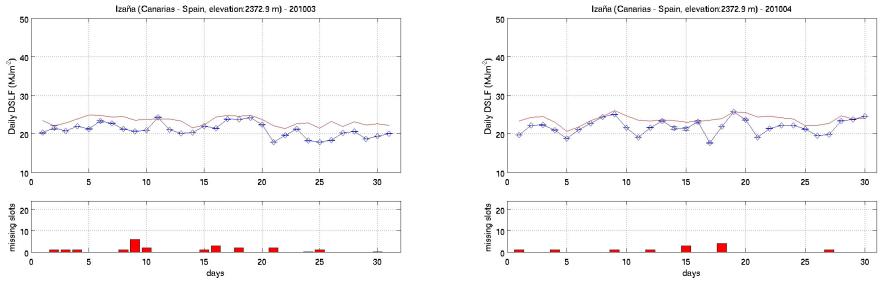
Izaña (Canarias - Spain, elevation:2372.9 m) - 201003
Daily DSLF (MJm-2)
missing slots
days

Izaña (Canarias - Spain, elevation:2372.9 m) - 201004
Daily DSLF (MJm-2)
missing slots
days

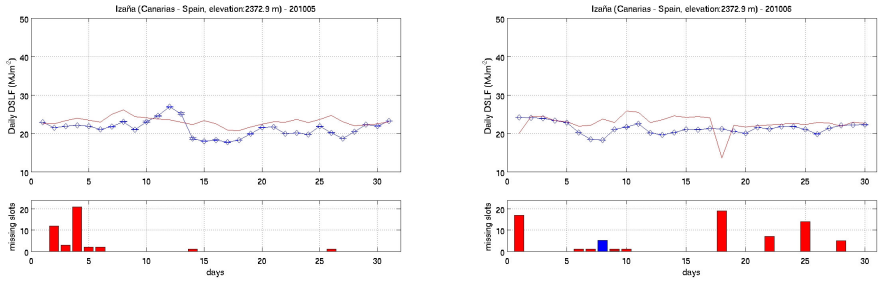
Izaña (Canarias - Spain, elevation:2372.9 m) - 201005
Daily DSLF (MJm-2)
missing slots
days

Izaña (Canarias - Spain, elevation:2372.9 m) - 201006
Daily DSLF (MJm-2)
missing slots
days

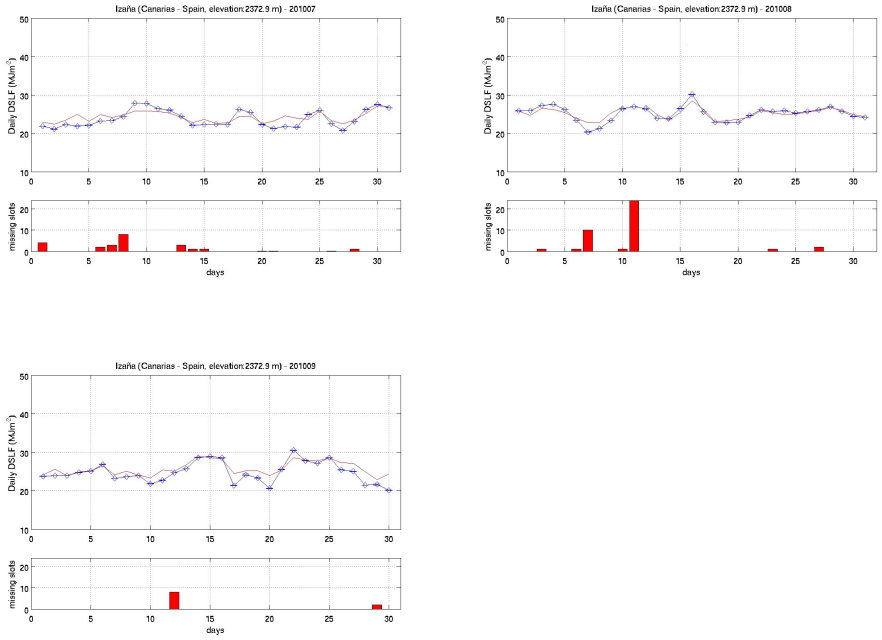

Figure 21 As in
Figure 16 but for Izaña

Table 9 As Table 7 but for Sede Boqer, Izaña and Tamanrasset stations

	SEDE BOQER				IZAÑA				TAMANRASSET			
	Mean Isitu MJm^{-2}	Mean SEVIRI MJ m^{-2}	Bias insitu-SEVIRI MJ m^{-2}	RMSD insitu-SEVIRI MJ m^{-2}	Mean Isitu MJm^{-2}	Mean SEVIRI MJ m^{-2}	Bias insitu-SEVIRI MJ m^{-2}	RMSD insitu-SEVIRI MJ m^{-2}	Mean Isitu MJm^{-2}	Mean SEVIRI MJ m^{-2}	Bias insitu-SEVIRI MJ m^{-2}	RMSD insitu-SEVIRI MJ m^{-2}
January	26	25	0.84	1.30	21	23	-1.78	2.51	24	22	1.60	26
February	27	26	1.03	1.64	22	24	-1.56	2.66	27	25	1.24	27
March	28	27	1.12	1.37	21	23	-2.28	2.63	27	25	1.93	28
April	28	27	0.58	1.01	22	24	-1.90	2.43	30	28	1.90	28
May	29	28	0.78	1.14	21	23	-1.83	2.67	32	29	2.22	29
June	31	29	1.61	2.90	21	23	-1.39	2.83				31
July					24	24	-0.39	1.37				
August					25	25	-0.06	0.93				
September					25	26	-1.02	1.69				

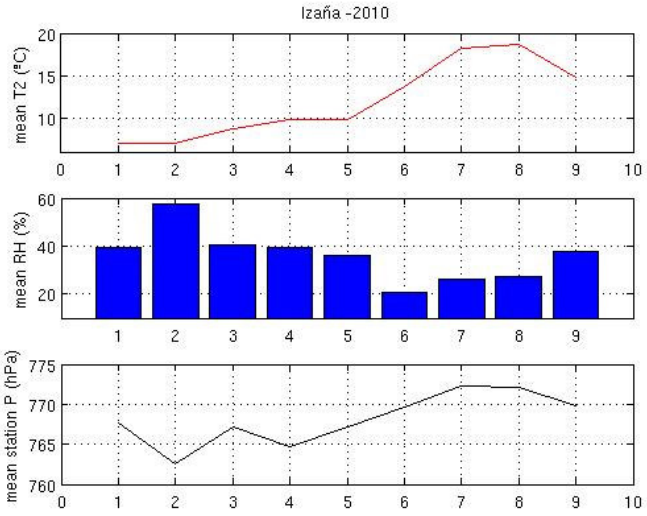

Figure 22 Monthly mean Temperature, relative humidity and surface pressure for Izaña from January 2010 to September 2010 obtained at Izaña BSRN station

Table 10 Number and percentage of pixels classification from SEVIRI cloud mask used on the instantaneous retrieval of DSLF for March 2010 and August 2010 at Izaña pixel.

	SEVIRI cloud mask					
	Clear		**Cloudy**		**Partially**	
March 2010	832	56.8%	410	27.9%	225	15.3%
August 2010	1399	94.8%	50	3.4%	27	1.8%

6 Concluding Remarks

The validation of DSLF values, generated by the LSA SAF algorithm used up to July 2009, suggests that a high percentage (generally over 60-to-70%) meets the target accuracy of 10% (Table 3). However, the results presented in section 3 also point towards a systematic underestimation of DSLF in clear sky conditions, and high dispersion of LSA SAF versus in situ measurements in cloudy and partially cloudy cases, with particularly poor results for Tamanrasset (Table 3).

A new algorithm, based on a modified version of the formulation first developed by Prata (1996) was then introduced in the SEVIRI/MSG operational chain in July 2009 and currently in use in the AVHRR/EPS parallel chain. The performance of this and a set of three other methods was verified against in situ data collected in several stations in Europe, one in the Middle East, and two in Africa (Figure 2). It is shown that part of the biases reported in section 3 are associated to differences between the station height and the ECMWF model surface orography. These may be partially eliminated through the application of an orography correction to the forecasts of 2m temperature and dew point. Nevertheless, the new Prata_modified algorithm improves the verification scores (bias and RMSE) for most cases, particularly for partially and totally cloudy cases.

The statistics of the different parameterizations of DSLF are compared with those of ECMWF model thermal infrared fluxes at the surface, for the same stations. The modified version of the Prata algorithm is able to reduce biases in ECMWF estimations for most stations, for both clear and cloudy sky conditions. The assessment of the different parameterization schemes for DLSF (section 4) supported the implementation of the Prata_modified algorithm in the SEVIRI/MSG operational chain in July 2009.

The validation of DIDSLF products indicates that generally more than 80% of the values meet the optimal to target accuracy (up to 10% relative errors; Table 6 and Table 8) for almost all stations. DIDSLF presented, however, larger discrepancies with observations taken at Toravere (Euro) and Izaña (NAfr). At Toravere the large satellite viewing angle combined with low solar zenith angles in winter makes pixel classification difficult. On top of this, temperature inversion and the presence of ice clouds further difficult the parameterization of thermal fluxes at the surface. DIDSLF product overestimates observations taken at Izaña from January to June. In this case, however, ground measurements are unlikely to be representative of nearby SEVIRI pixels, since the station is often above the layer of stratocumulus clouds. In both stations the systematic deviations between ground measurements and satellite retrievals are detected for instantaneous values of DSLF, which are then propagated to the daily accumulated values.

The quality of the daily DSLF product essentially mirrors that of DSLF_SEVIRI (sections 3 and 4). High errors may occur for days with a high percentage of missing instantaneous DSLF fields. However, these are clearly flagged in the final product, since the statistics on available data are added as an extra dataset. When compared to ECMWF forecast, LSA SAF values show similar ranges and intra-annual variability. The main field patterns are also recognisable both datasets. The LSA SAF daily DSLF tends to overestimate ECMWF values, although discrepancies are generally within 10-to-20 Wm^{-2}. Strong underestimation, when compared with ECMWF values, is obtained

over high latitudes winter. Under such conditions, the performance of both ECMWF and LSA SAF thermal flux estimations require further investigation.

7 References

Berk, A., G.P. Anderson, P.K. Acharya, J.H. Chetwynd, L.S. Bernstein, E.P. Shettle, M.W. Matthew, and S.M. Alder-Golden, (2000): "MODTRAN4 Version 2 User's Manual Air Force Res. Lab.", Space Vehicles Directorate, Air Force Material Command, Hanscom AFB, MA, 2000.

Chevallier, F., (2001): Sampled databases of 60-level atmospheric profiles from the ECMWF analyses. Numerical Weather Prediction Satellite Application Facility *Research Report* [NWP SAF Res. Rep.] no. 4, available at http://www.ecmwf.int

Crewel, S., M. Drusch, E. van Meijgaard, and A. van Lammeren (2002), Cloud observations and modelling within the European BALTEX Cloud Liquid Water network. *Boreal Environ. Res.*, **7**, 235-245.

Dilley, A.C. and D.M. O'Brien (1998): Estimating downward clear sky long-wave irradiance at the surface from screen temperature and precipitable water, *Q. J. R. Meteorol. Soc.*, **124**, 1391-1401.

Josey, S.A., Pascal, R.W., Taylor, P.K., Yelland, M.J., (2003): A New Formula For Determining the Atmospheric Longwave Flux at Ocean Surface at Mid-High Latitudes. *J Geophys. Res.*, doi:10.1029/2002JC00141.

Meetschen, D., B. J. J. M. van den Hurk, F. Ament, and M. Drusch (2004), Optimized surface radiation fields derived from Meteosat imagery and a regional atmospheric model. *J. Hydromet.*, **5**, 1091-1101.

Morcrette, J.-J. (2001), The surface downward longwave radiation in the ECMWF forecast system. *Technical Memorandum no. 339*, ECMWF, Reading, 34 pp., available at http://www.ecmwf.int

Prata, A.J. (1996): A new long-wave formula for estimating downward clear-sky radiation at the surface, *Q. J. R. Meteorol. Soc.*, **122**, 1121-1151.

Slingo, A., T. P. Ackerman, R. P. Allan, E. I. Kassianov, S. A. McFarlane, G. J. Robinson, J. C. Barnard, M. A. Miller, J. E. Harries, J. E. Russell, and S. Dewitte (2006), Observations of the impact of a major Saharan dust storm on the atmospheric radiation balance, *Geophys. Res Lett.*, **33, L24817**, doi:10.1029/2006GL027869.

Trigo, I. F., C. Barroso, P. Viterbo, Sandra C. Freitas and Isabel T. Monteiro (2010), Estimation of downward long-wave radiation at the surface combining remotely sensed data and NWP data, *J Geophys. Res.*, doi:10.1029/2010JD013888.

Wild, M., A. Ohmura, H. Gilgen, and E. Roeckner (1995), Validation of general circulation model radiative fluxes using surface observations. *J. Clim.*, **8**, 1309-1324.